

Empirical Improvements for Estimating Earthquake Response Spectra with Random-Vibration Theory

By David M. Boore and Eric M. Thompson

Abstract

The stochastic method of ground-motion simulation is often used in combination with random-vibration theory to directly compute ground-motion intensity measures, thereby bypassing the more computationally intensive time-domain simulations. Key to the application of random-vibration theory to simulate response spectra is determining the duration (D_{rms}) used in computing the root-mean-square oscillator response. Boore and Joyner (1984) originally proposed an equation for D_{rms} , which was improved by Liu and Pezeshk (1999). Though these equations are both substantial improvements over using the duration of the ground-motion excitation for D_{rms} , we document systematic differences between the ground-motion intensity measures derived from the random-vibration and time-domain methods for both of these D_{rms} equations. These differences are generally less than 10% for most magnitudes, distances, and periods of engineering interest. Given the systematic nature of the differences, however, we feel that improved equations are warranted. We empirically derive new equations from time-domain simulations for eastern North America and western North America seismological models. The new equations improve the random-vibration simulations over a wide range of magnitudes, distances, and oscillator periods.

Introduction

The stochastic method (Boore, 2003) is widely used for simulation of seismic ground-motion intensity measures (GMIMs), such as peak acceleration and response

spectral amplitudes, particularly for regions lacking strong-motion recordings for magnitudes and distances of engineering interest. Recent applications include the ongoing PEGASOS project in Switzerland (Abrahamson *et al.*, 2002; Renault *et al.*, 2010) and the Pacific Earthquake Engineering Research Center's Next Generation Attenuation—East (NGA-E) project (see Data and Resources section). The GMIMs can be simulated using either time-domain simulations or random-vibration simulations, given the model describing the Fourier spectrum of ground motion (this spectrum includes source radiation effects and the amplitude changes due to propagation from the source to the site) and a description of the duration of ground shaking at the site (which is made up of source and path contributions—this duration of excitation is denoted here as D_{ex}). Random-vibration simulations are usually thousands of times faster than time-domain simulations, which is important for computationally intensive applications, such as inverting data for model parameters (Scherbaum *et al.*, 2006) or simulating the probability density distribution of GMIMs by Monte Carlo simulations that sample the probability distributions of the model parameters.

Although the calculations are much quicker, there is a potential fundamental problem with random-vibration simulations: the basic assumptions behind random-vibration calculations, such as quasi-stationarity of the equivalent time series and the statistical independence of consecutive maxima of the time series, are not obviously satisfied, particularly for long-period GMIMs. To overcome these limitations, modifications to the random-vibration simulations in which two measures of duration are used were proposed by Boore and Joyner (1984) (BJ84). The measure of most concern to us is D_{rms} , the duration used to compute the root-mean-square of the oscillator response. BJ84 introduced an equation for D_{rms} , and Liu and Pezeshk (1999) (LP99), using BJ84 as the starting point, proposed a different equation. Both the BJ84 and the LP99 equations were based on comparisons of time-domain and random-vibration simulations for the same model, as well as some theoretical considerations. The

adequacy of those modifications, however, was demonstrated only for a few magnitudes and distances, using comparisons of response spectra plotted using a log scale for the ordinate. We recently had occasion to look more carefully at the comparisons for a wide range of magnitudes and distances, using ratios of time-domain (TD) and random-vibration (RV) simulations. An example is shown in Figure 1. The stochastic simulations were generated with the SMSIM software (Boore, 2005). The model parameters are given in Table 1 and in the electronic supplement to this paper, as discussed later. As shown in Figure 1, the results using the LP99 equation are generally better than those using the BJ84 equation, and both are generally much better than using D_{ex} in computing the root-mean-square of the oscillator response, particularly for M 6 and greater. In spite of the improvements using the equations introduced by BJ84 and LP99, there are significant discrepancies from the TD results (which we take to be the correct GMIMs, given the assumed seismological model), particularly at long periods. There is also a consistent, but small, bias at short periods that is essentially independent of magnitude and distance. These discrepancies are hard to see on traditional plots of GMIMs using a log scale for the ordinate because the GMIMs span a wide range of amplitudes as a function of period for a given magnitude and distance. In this article we evaluate the existing D_{rms} equations for more magnitudes and distances than were originally used to derive these equations, and from these results we provide improvements to the D_{rms} equations for several stochastic-method models. We start with a brief review of the RV method as used in the stochastic method developed by Boore (1983, 2003). This is followed by the main section containing the improved equation for D_{rms} .

Review of Random-Vibration Simulations

As discussed in Boore (1983, 2003), the RV simulations are based on two things: 1) the root-mean-square of the GMIM (y_{rms}), obtained through Parseval's theorem from the seismological-dependent model of the Fourier amplitude spectrum, and 2) a peak-to-

rms factor ($p = y_{max}/y_{rms}$), relating the peak GMIM (y_{max}) to y_{rms} . In this article we compute p using the equations given by Boore (2003), which are based on equation (6.8) in Cartwright and Longuet-Higgins (1956). Another method for computing p is given by Der Kiureghian (1980). We have compared GMIMs from both methods and do not find that one is better than the other; for the sake of consistency, the oscillator modifications given in this paper should be used with the Boore (2003) computation of p .

Boore and Joyner (1984) introduced a modification in the RV method for computing response spectra by using different duration measures in computing p and y_{rms} . The duration of ground motion, D_{ex} , is used in computing p , while y_{rms} is computed using a modification of D_{ex} that accounts for the increase in duration due to oscillator response; this duration is termed D_{rms} . This article is fundamentally concerned with computing D_{rms} as a function of magnitude, distance, oscillator period, and the seismological model.

A New Equation for Computing D_{rms}

A useful equation for determining the D_{rms} that will provide agreement between TD and RV simulations for a given set of model parameters, including oscillator period, magnitude, and distance, is easily derived from the definitions of y_{rms} and the rms-to-peak factor p . From Parseval's theorem,

$$y_{rms} = \sqrt{m_0/D_{rms}}, \quad (1)$$

where m_0 is the zeroth spectral moment (e.g., Boore, 2003) and D_{rms} is the duration to be used in computing y_{rms} . From the definition of p given in the Review of Random-Vibration Simulations section, we have

$$y_{max} = p \times y_{rms} . \quad (2)$$

As discussed before, p depends on D_{ex} , the duration of ground motion, not the duration of the oscillator response. Now consider two estimates of y_{max} , one from the TD simulation (assumed to be the correct value) and one from the RV simulation with no adjustment to account for the oscillator-response (i.e., $D_{rms} = D_{ex}$). Call them y_{td} and y_{xo} , respectively. Equations (1) and (2) give

$$y_{td} = p \times \sqrt{m_0 / D_{rms}} , \quad (3)$$

and

$$y_{xo} = p \times \sqrt{m_0 / D_{ex}} . \quad (4)$$

Because p is the same in both equations, equations (3) and (4) can be solved for the value of D_{rms} that will give the correct value of ground motion when used in the RV simulations:

$$D_{rms} = D_{ex} (y_{xo} / y_{td})^2 \quad (5)$$

or

$$D_{rms} / D_{ex} = (y_{xo} / y_{td})^2 . \quad (6)$$

To illustrate the use of equation (6) we generated both TD and RV simulations for the models given in Table 1 and the parameter input files contained in the electronic

supplement to this paper. We used the SMSIM software (Boore, 2005) for the simulations. The base model for the illustrations in this article is the eastern North America (ENA) single-corner-frequency (SCF) model (we used this model because an important application of the stochastic method is in deriving ground-motions in ENA, as in the ongoing NGA-E project). For each magnitude--distance pair, we use the arithmetic mean of the response spectra of 800 TD simulations as the TD GMIM (we found such a large number was necessary to obtain relatively smooth PSA when plotted vs. period). The motions in Figure 1 considered a range of stress parameters (a factor of four on either side of 250 bars), and the results show that the TD/RV ratio is not sensitive to the stress parameter. For that reason we used 250 bars (see Boore, 2009) and generated y_{td} and y_{xo} for many values of magnitude, distance, and oscillator period. The results are shown in Figure 2, where $D_{rms}/D_{ex} = (y_{xo}/y_{td})^2$ is plotted against both oscillator period, T_o , and the normalized oscillator period T_o/D_{ex} for one distance and many magnitudes (top row) and one magnitude and many distances (bottom row). Using the normalized oscillator period removes much of the apparent variability in D_{rms}/D_{ex} , suggesting that a relatively simple functional form in terms of T_o/D_{ex} can be found that will improve on the BJ84 and LP99 equations for D_{rms} .

Functional Form

The general form of the equation used by BJ84 and LP99 to obtain D_{rms} is

$$D_{rms} = D_{ex} + D_o \left(\frac{\gamma^n}{\gamma^n + \alpha} \right) \quad (7)$$

where $\gamma = D_{ex}/T_o$. D_o is the oscillator duration $T_o/2\pi\zeta$, where ζ is the fractional damping of the oscillator--usually 0.05. As we saw in Figure 2, T_o/D_{ex} rather than T_o is a better predictor variable for D_{rms}/D_{ex} . For this reason, we rewrite equation (7) as

$$D_{rms}/D_{ex} = 1 + \frac{1}{2\pi\zeta} \left(\frac{\eta}{1 + \alpha\eta^n} \right), \quad (8)$$

where $\eta = T_o/D_{ex}$. BJ84 recommend $n = 3$ and $\alpha = 1/3$. LP99 recommend $n = 2$ and that α be determined from an equation that accounts for spectral shape. Equation (8) has the property that D_{rms}/D_{ex} approaches unity for small and large values of η , for $n > 1$.

These are physical constraints that follow from the oscillator time series being proportional to ground acceleration and ground displacement at short and long periods, respectively, and therefore the duration of the oscillator response will be equal to the duration of the ground motion at these asymptotic values of period. But Figure 2 shows that D_{rms}/D_{ex} does not always approach unity, and in many cases approaches a different value as η approaches zero than when η approaches infinity. D_{rms}/D_{ex} is given by the ratio of random-vibration to time-domain simulations (equation (6)), and thus the fact that D_{rms}/D_{ex} does not approach the theoretical value of unity indicates a bias between the RV and TD simulations. To allow for the empirical observation that D_{rms}/D_{ex} does not approach unity for small and large values of η , we add a term to equation (8) to get

$$D_{rms}/D_{ex} = \left(c_1 + c_2 \frac{1 - \eta^2}{1 + \eta^2} \right) \left[1 + \frac{1}{2\pi\zeta} \left(\frac{\eta}{1 + \alpha\eta^n} \right) \right], \quad (9)$$

which approaches $c_1 + c_2$ as η approaches zero and $c_1 - c_2$ as η approaches infinity.

This equation is still not general enough to capture the range in shapes of D_{rms}/D_{ex} that we observe, so we further generalize the equation by allowing α and n to be free coefficients (c_5 and c_6) to be estimated from the data and by adding three more coefficients (c_3 , c_4 , c_7):

$$D_{rms}/D_{ex} = \left(c_1 + c_2 \frac{1 - \eta^{c_3}}{1 + \eta^{c_3}} \right) \left[1 + \frac{c_4}{2\pi\zeta} \left(\frac{\eta}{1 + c_5\eta^{c_6}} \right)^{c_7} \right]. \quad (10)$$

This is the equation which we fit to the simulated D_{rms}/D_{ex} ratio, with a set of coefficients for each magnitude and distance.

Estimation of the Coefficients

We used the SMSIM programs `tmrs_loop_rv_drvr` and `tmrs_loop_td_drvr` to generate GMIMs for a set of 15 distances logarithmically spaced from 2 km to 1262 km and nine magnitudes linearly spaced from 4 to 8. For each magnitude--distance pair we computed PSA at 200 logarithmically spaced periods, for 5% damping. We do not provide coefficients for other damping levels because we prefer to use correlations of PSA for various damping levels, such as those of Cameron and Green (2007) and those being developed for the PEER NGA-W2 project (see Data and Resources section), that can be used to adjust for simulations of PSA for other levels of damping. We computed D_{rms}/D_{ex} for several ENA and WNA models, including single-corner frequency models and double-corner frequency models. An additional consideration is the low-cut filter; we simulated the GMIMs with no low-cut filter and with a low-cut filter frequency (f_{lc}) of 0.03. The base case that we use to illustrate this article is the single-corner frequency model for ENA with no low-cut filter. The D_{rms}/D_{ex} ratio depends on whether a box or an exponential window is used in the TD simulations. Because we think that most users prefer the more realistic look of the acceleration time series computed using the exponential window, we only report coefficients for the exponential time-domain window of Saragoni and Hart (1974). This was also the window used for the simulations on which the BJ84 and LP99 equations were based.

Given the complex functional form of equation (10), the interdependence of the parameters, and the restricted range of possible values that the parameters may take, we

decided to use a genetic algorithm (GA) to search the parameter space for the best values of the coefficients. Given the insensitivity to stress, we defined the misfit relative to D_{rms}/D_{ex} for a single representative stress value for each region (100 bars for WNA; 250 bars for ENA). The range of allowable values for the coefficients are listed in Table 2 (based on exploratory calculations, we decided to constrain c_3 to the value 2.0). The genetic algorithm uses 256 for the population size and the maximum number of generations. For each magnitude-distance bin we computed two GA estimates of the coefficients, using two seeds to generate initial populations of models, selecting the GA estimate leading to the best fit as the final estimate (except for the first magnitude-distance bin, which used the coefficients that simplify equation 10 to the BJ84 equation). The two estimates were 1) using the coefficients from the previous magnitude at the same distance, and 2) using the previous distance at the same magnitude. We derived coefficients for equation (10) from simulations for the two base-case single-corner frequency models for ENA and WNA, with the coefficients given in the electronic supplement to this paper. We validated these equations at the midpoints between the magnitudes and distances where the coefficients are defined (geometric midpoints for distance) and found no increase in the misfit to D_{rms}/D_{ex} . For magnitude and distance values not in the coefficient tables, we first compute D_{rms}/D_{ex} for the four tabulated moment magnitude (**M**) and distance (**R**) pairs surrounding the desired **M** and **R**, and then use bilinear interpolation to obtain D_{rms}/D_{ex} .

Some Results Using the New Equation

A sample of the simulated and fitted D_{rms}/D_{ex} ratios is given in Figure 3, along with D_{rms}/D_{ex} from the BJ84 and LP99 methods for computing D_{rms} . The TD/RV ratios obtained using the new computations of D_{rms} (BT12) are shown in Figure 4, which is the same as Figure 1 with the addition of the RV simulations using the BT12 computations. Figure 5 displays a different way of showing the comparison, using shaded contour plots

for a wide range of periods and distances for a set of magnitudes and methods for computing D_{rms} . As shown in the figure, using $D_{rms} = D_{ex}$ in the RV simulations will give good agreement with the TD simulations only for restricted (and correlated) regions of distance and period. Both the BJ84 and the LP99 equations result in improvements over no modification to D_{rms} and lead to values within about 10% of the TD simulations for periods ranging from less than about 1 s for **M** 4 to periods less than 100 s or longer for **M** 8. The results of using the LP99 equation are the same as using the BJ84 equation for short periods, but differ for longer periods, for which RV simulations using the LP99 equation are closer to the TD simulations than the RV simulations that use the BJ84 equation. Because engineering applications are often concerned with periods less than one or two seconds, Figure 5 suggests that the BJ84 and the LP99 equations will give reasonable results in many cases. But the new equation (BT12, after the authors' last initials and presumed year of publication of this article) leads to a significant improvement in the RV simulations compared to the BJ84 and LP99 computations over a wide range of magnitudes, distances, and periods, and as the new equation is easy to implement, we recommend its use over the previous equations for determining D_{rms} in RV simulations.

Using D_{rms} Computations in Models for Which the Coefficients were not Derived

The results in Figure 5 for the BT12 calculations are a consistency check that the computations were done correctly, because the coefficients in the equation for D_{rms} were designed to match the TD simulations for this model (the SCF ENA model, with no low-cut filter). The good agreement between the TD and the RV simulations says nothing

about the applicability of the BT12 coefficients used in Figure 5 for RV simulations based on other models. We address that in this section by comparing TD and RV simulations for other models for which the BT12 coefficients were not derived, but using equation (10) with the base-case ENA and WNA BT12 coefficients to compute D_{rms} in the RV simulations. We consider single-corner frequency and double-corner frequency models for both ENA and WNA (Table 1), and for each source model we consider two models, one with no low-cut filter and one with a low-cut filter of 0.03 Hz, for a total of eight models. The best way to appreciate the differences in the ground-motion models is to look at the Fourier acceleration spectra (FAS) for representative magnitudes and distances. These are shown in Figure 6. The differences in low-frequency amplitudes for the ENA and WNA models are primarily due to the differences in geometrical spreading ($1/R^{1.3}$ for ENA and $1/R$ for WNA); these differences are not important for the RV vs. TD comparison because geometrical spreading does not affect the shape of the FAS. Of much more importance are the other differences in the models, including whether the source spectra have one or two corner frequencies, the whole-path attenuation parameter $Q(f)$, and the high-frequency diminution parameter κ_0 . This latter parameter is very different in the ENA and WNA models (0.005 s and 0.030 s, respectively), and this leads to the pronounced differences in the high-frequency FAS at close distances.

Comparisons of the RV and TD simulations for the ENA models that were not used in deriving the BT12 coefficients for ENA are shown in Figure 7. The top row of graphs is for the SCF model with a low-cut filter of 0.03 Hz. The mismatch between TD and RV is only important for periods greater than the filter period (33 s) and becomes increasingly important as magnitude increases (because larger earthquakes have relatively more long-period energy than small earthquakes and thus the long-period oscillator response will be more sensitive to low-cut filtering). The next two rows of graphs in Figure 7 are for the double-corner ENA model, without and with a low-cut filter. As before, the new modifications work well for shorter periods, with significant

differences only for longer periods. The lesson from Figure 7 is that for most cases of interest (periods less than about 10 s), the BT12 coefficients derived from the SCF, no low-cut filter case work well. A similar conclusion holds for the WNA models (see the electronic supplement to this paper, in which TD and RV ratios are shown for four models, similar to those used for ENA: SCF and double corner frequency, without and with low-cut filtering).

A harsher test of the applicability of the new equation for D_{rms} is to use the equation with coefficients from the ENA model in RV predictions of motions for a WNA model, and vice versa (note that the spectral moments for the RV simulations will be computed from the correct ground-motion model; it is only the D_{rms} computation that mixes models). The results of doing this are shown in the top two rows of Figure 8, for the SCF ENA and WNA models. Except for the smallest earthquake (at periods that increase with distance), the “wrong” coefficients work quite well. This led us to consider using an average of the D_{rms} computed for the ENA and WNA coefficients in the RV simulations (i.e., BT12-combined); the results of doing that are shown in the bottom two rows of Figure 8. In general, the comparison with the TD simulations is now quite good. It clearly is impossible to sample all possible models, but we feel that these models encompass a wide range of the models currently in use.

Discussion and Conclusions

Using time-domain and random-vibration simulations for response spectra over a wide range of periods, magnitudes, and distances, we first evaluated existing equations for the determination of the duration (D_{rms}) used to compute root-mean-square accelerations in random-vibration (RV) stochastic-method simulations; these equations are those of Boore and Joyner (1984) (BJ84) and Liu and Pezeshk (1999) (LP99). We found that the LP99 equation generally works better than that of BJ84, and that the RV simulations using the BJ84 and the LP99 equations are within about 10% of the time-domain simulations for magnitudes, distances, and periods of most engineering interest ($M \gtrsim 5$, $R \gtrsim 10$ km, and $T \lesssim 2$ s for $M 5$, increasing to more than 100 s for $M 8$). There is considerable variability of the ratio of TD to RV simulations in this range, however. To improve the RV simulations we derived a new equation for the computation of D_{rms} . The new equation for computing D_{rms} leads to better agreement with TD than using the previous equations for D_{rms} throughout a large range of magnitudes, distances, periods, and seismological models. The improvements are particularly effective for small magnitudes and long periods, but they also remove a small but persistent bias at short periods. Using the new equation adds only a negligible increase in computational time; even with the new equation the RV simulations are thousands of times faster than the TD simulations. A fundamental factor in the relatively long computational time for the TD simulations is that many simulations are needed to produce relatively smooth response spectra—we used 800 simulations for each magnitude and distance in this article. In addition, the small value of the diminution parameter κ_0 for the ENA models results in richer content of high-frequency ground motions for ENA than for WNA, and this increased high-frequency content requires a much smaller time step in the ENA time-domain simulations, which substantially increases the time required to generate a time series (we use $dt = 0.001$ s for ENA and $dt = 0.005$ s for WNA).

The coefficient tables we provide for the computation of D_{rms} were generated for TD simulations using an exponential time window, rather than a box window (the BJ84 and LP99 modifications also used an exponential window), and the rms-to-peak factors were those discussed in Boore (2003), from Cartwright and Longuet-Higgins (1956), rather than an alternative such as Der Kiureghian (1980). For consistency, any comparisons of TD and RV results should use these stochastic-model parameters.

Two sets of coefficients for the new equation for D_{rms} are provided, one for a standard eastern North America (ENA) model and one for a standard western North America (WNA) model. The models differ in many particulars, the most important for this article being the value of κ_0 : 0.005 s for ENA and 0.030 s for WNA. Although the coefficients depend on the particular model for which they were derived, we find that in general the RV simulation results are not too sensitive to which set of coefficients is used. The exception to this is for very long periods, large distances, and small magnitudes, which do not control the hazard for most earthquake hazard analyses. We recommend using the set of coefficients from the model closest to the one under consideration. In particular, models with very small values of κ_0 should use the ENA coefficients, while those with larger values should use the WNA coefficients. For intermediate values of κ_0 , the average of D_{rms} computed from the ENA and the WNA coefficients can be used in the RV simulations. Of course, it is good practice to spot check the RV and the TD simulations for situations in which the ground-motion models are not similar to either of those used here.

Data and Resources

The latest version of the SMSIM programs used for the simulations can be obtained from the online software link on <http://www.daveboore.com> (last accessed

October, 2011); their use is described in Boore (2005). Version 3.29 (and higher) of SMSIM contains the coefficient files for the “default” D_{rms} coefficients (based on single-corner frequency ENA and WNA models, with no low-cut filter), and the random vibration programs and the parameter files have been modified to make use of these coefficients. The genetic algorithm calculations were done using the R package rgenoud (Mebane and Sekhon, 2011), obtainable from <http://www.r-project.org/> (last accessed October, 2011). A description of the NGA-E project is given in <http://peer.berkeley.edu/ngaeast/> (last accessed October, 2011), and the NGA-W2 task for developing damping modifications is discussed in <http://peer.berkeley.edu/ngawest2/tasks/task-6-damping-scaling/> (last accessed October, 2011).

Acknowledgments

We thank John Douglas, Rob Graves, Jim Kaklamanos, and two anonymous reviewers for their thoughtful comments and suggestions.

References

- Abrahamson, N. A., Birkhauser, P., Koller, M., Mayer-Rosa, D., Smit, P., Sprecher, C., Tinic, S., and Graf, R. (2002). PEGASOS: A comprehensive probabilistic seismic hazard assessment for nuclear power plants in Switzerland, in *Proceedings, 12th European Conference on Earthquake Engineering*, paper 633, London.
- Atkinson, G. M. (2004). Empirical attenuation of ground-motion spectral amplitudes in southeastern Canada and the northeastern United States, *Bull. Seism. Soc. Am.* **94**, 1079--1095.
- Atkinson, G. M. and D. M. Boore (1995). Ground-Motion Relations for Eastern North America, *Bull. Seism. Soc. Am.* 85, 17-30.

- Atkinson, G. M. and D. M. Boore (2006). Earthquake Ground-Motion Prediction Equations for Eastern North America, *Bull. Seism. Soc. Am.* 96, 2181-2205.
- Atkinson, G. M. and W. Silva (2000). Stochastic modeling of California ground motions, *Bull. Seismol. Soc. Am.* **90**, 255—274.
- Boore, D. M. (1983). Stochastic simulation of high-frequency ground motions based on seismological models of the radiated spectra, *Bull. Seismol. Soc. Am.* **73**, 1865—1894.
- Boore, D. M. (2003). Simulation of ground motion using the stochastic method, *Pure Appl. Geophys.* 160, 635-676.
- Boore, D. M. (2005). SMSIM---Fortran Programs for Simulating Ground Motions from Earthquakes: Version 2.3---A Revision of OFR 96-80-A, U.S. Geological Survey Open-File Report, *U. S. Geological Survey Open-File Report 00-509*, revised 15 August 2005, 55 pp.
- Boore, D. M. (2009). Comparing stochastic point-source and finite-source ground-motion simulations: SMSIM and EXSIM, *Bull. Seismol. Soc. Am.* **99**, 3202-3216.
- Boore, D. M., and W. B. Joyner (1984). A note on the use of random vibration theory to predict peak amplitudes of transient signals, *Bull. Seism. Soc. Am.* 74, 2035-2039.
- Cameron, W. I. and R. A. Green (2007). Damping correction factors for horizontal ground-motion response spectra, *Bull. Seismol. Soc. Am.* **97**, 934-960.
- Cartwright, D. E. and M. S. Longuet-Higgins (1956). The statistical distribution of the maxima of a random function, *Proc. R. Soc. London* 237, 212–232.
- Der Kiureghian, A. (1980). Structural response to stationary excitation, *J. of Engineering Mechanics Division* **EM6**, 1195-1213.

Liu, L. and S. Pezeshk (1999). An Improvement on the Estimation of Pseudoresponse Spectral Velocity Using RVT Method, *Bull. Seismol. Soc. Am.* **89**, 1384–1389.

Mebane, Jr., W. R. and J. S. Sekhon (2011). Genetic Optimization Using Derivatives: The rgenoud package for R, *J. of Statistical Software* **42**, 1-26.

Raof, M. R. B. Herrmann, and L. Malagnini (1999). Attenuation and excitation of three-component ground motion in Southern California, *Bull. Seismol. Soc. Am.* **89**, 888-902.

Renault, P., S. Heuberger, N. A. Abrahamson (2010). PEGASOS Refinement Project: An improved PSHA for Swiss nuclear power plants, *Proceedings, 14th European Conference on Earthquake Engineering*, paper 991, available from <http://www.dist.unina.it/proc/2010/14ECEE/Data/PDF/991.pdf> (last accessed October 2011).

Saragoni, G. R. and G. C. Hart (1974). Simulation of Artificial Earthquakes, *Earthq. Eng. Struct. Dyn.* **2**, 249–267.

Scherbaum, F., F. Cotton, and H. Staedtke (2006). The estimation of minimum-misfit stochastic models from empirical ground-motion prediction equations, *Bull. Seismol. Soc. Am.* **96**, 427–445, doi: 10.1785/0120050015.

Contact Information

U.S. Geological Survey

MS 977

345 Middlefield Road

Menlo Park, CA 94025

boore@usgs.gov

(D.M.B.)

Tufts University

113 Anderson Hall

Medford, MA 02155

eric.thompson@tufts.edu

(E.M.T.)

Tables

Table 1. Essential differences in the stochastic-method models used in the simulations discussed in this paper.*

Model	Source	Path Attenuation	Path Duration	κ (s)
ENA: SCF	Single corner frequency	Atkinson (2004)	Atkinson & Boore (2006)	0.005
ENA: AB95	Double corner frequency (Atkinson & Boore, 1995)	Atkinson (2004)	Atkinson & Boore (2006)	0.005
WNA: SCF	Single corner frequency	Raof <i>et al.</i> (1999)	0.05R	0.030
WNA: AS00	Double corner frequency (Atkinson & Silva, 2000)	Raof <i>et al.</i> (1999)	0.05R	0.030

* See the electronic supplement to this paper for the parameter files used in the simulations.

Table 2. The range of the parameters in equation (10) used in the genetic algorithm.

Parameter	Minimum	Maximum
c_1	0.7	1.2
c_2	-0.6	0
c_3	2	2
c_4	0	3
c_5	0	50
c_6	1	10
c_7	0	10

Figure Captions

Figure 1. Ratios of the PSA computed from TD simulations to the PSA computed with RVT using the BJ84 and LP99 D_{rms} equations for different magnitudes and distances, using the ENA model given in Table 1 with no low-cut filter. Also shown is the TD/RV ratio when $D_{rms} = D_{ex}$ (i.e., no RV modification to account for the oscillator response). The ordinate scale was chosen deliberately to emphasize the results using BJ84 and LP99, at the expense of truncating the TD/RV ratios for the $D_{rms} = D_{ex}$ case, which have minimum values near 0.6. Note that the shaded region encompasses the range of ratios obtained for three different stresses: 62.4, 250, and 1000 bars.

Figure 2. Squared ratios of PSA from random-vibration simulations (for which $D_{rms} = D_{ex}$) and time-domain simulations, for the ENA SCF model in Table 1 with 250 bar stress parameter and no low-cut filter, plotted against period (T_o) and period normalized by the duration of excitation (T_o/D_{ex}). The top row shows ratios for a fixed distance (20 km) and a suite of magnitudes; the bottom row shows ratios for a fixed magnitude (6.5) and a suite of distances.

Figure 3. Plots of D_{rms}/D_{ex} as estimated from equation (6) (i.e., $(y_{xo}/y_{td})^2$) as a function of $\eta = T_o/D_{ex}$ for the same \mathbf{M} , \mathbf{R} , and stresses as Figure 1. The BT12 curves are from equation (10) with coefficients derived from fitting the D_{rms}/D_{ex} values derived from the TD and RV simulations. The BJ84 and LP99 curves are from equation (8), with the coefficients recommended by the respective authors.

Figure 4. Same as Figure 1 with the addition of the ratios computed using the D_{rms} equation proposed in this article (BT12).

Figure 5. A shaded contour plot of the TD/RV ratios for the ENA SCF 250 bar, no low-cut filter model, for $D_{rms} = D_{ex}$ (no modification for an oscillator) (top row), and the following models for calculating the D_{rms} used in the RV simulations: BJ84 (second row), LP99 (third row), and BT12 (bottom row). The results of using the BT12 calculations of D_{rms} look blank because the ratios are within $\pm 5.3\%$ of unity.

Figure 6. Fourier acceleration spectra (FAS) for models used in this article (see Table 1 and the electronic supplement to this paper), for selected magnitudes and distances.

Figure 7. A shaded contour plot of the TD/RV ratios for various ENA models not used to derive the coefficients used in the BT12 D_{rms} computations (see Table 1 and the electronic supplement to this paper for model details). The base-case ENA BT12 coefficients were used in these comparisons. (top row): ENA SCF 250 bar model with a 0.03 Hz low-cut filter. (middle row): ENA AB95 two-corner model, no low-cut filter. (bottom row): ENA AB95 two-corner model, 0.03 Hz low-cut filter.

Figure 8. A shaded contour plot of the TD/RV ratios for various ENA and WNA models not used to derive the coefficients used in the BT12 D_{rms} computations (see Table 1 and the electronic supplement to this paper for model details). (top row): ENA SCF 250 bar model with no low-cut filter, using D_{rms} computed from the BT12 WNA coefficients. (second row): WNA SCF 100 bar model with no low-cut filter, using D_{rms} computed from the BT12 ENA coefficients. (third row): ENA SCF 250 bar model with no low-cut filter, using an average of D_{rms} computed from the BT12 ENA and WNA coefficients. (bottom row): WNA SCF 100 bar model with no low-cut filter, using an average of D_{rms} computed from the BT12 ENA and WNA coefficients.

Figures

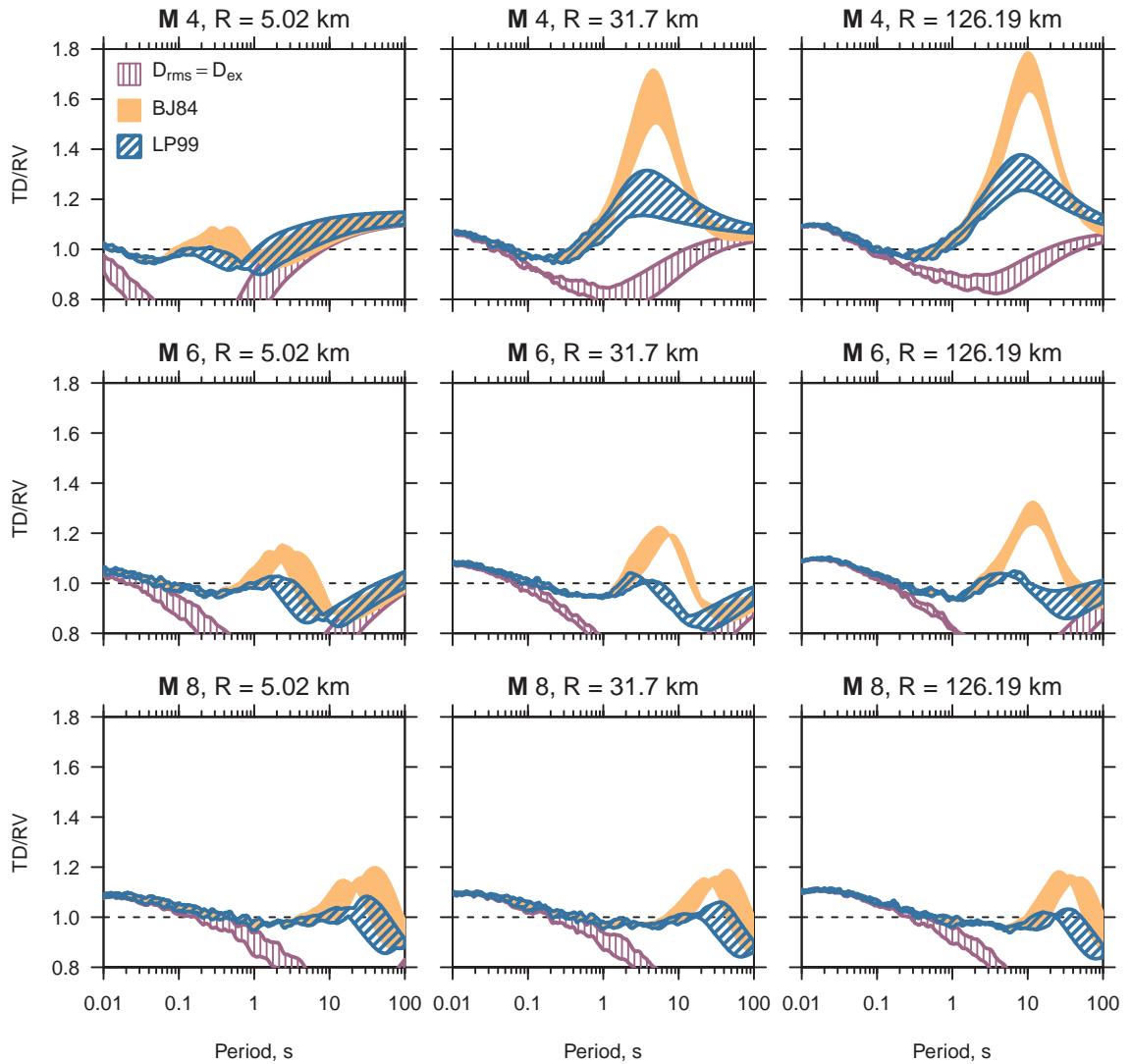


Figure 1. Ratios of the PSA computed from TD simulations to the PSA computed with RVT using the BJ84 and LP99 D_{rms} equations for different magnitudes and distances, using the ENA model given in Table 1 with no low-cut filter. Also shown is the TD/RV ratio when $D_{rms} = D_{ex}$ (i.e., no RV modification to account for the oscillator response). The ordinate scale was chosen deliberately to emphasize the results using

BJ84 and LP99, at the expense of truncating the TD/RV ratios for the $D_{rms} = D_{ex}$ case, which have minimum values near 0.6. Note that the shaded region encompasses the range of ratios obtained for three different stresses: 62.4, 250, and 1000 bars.

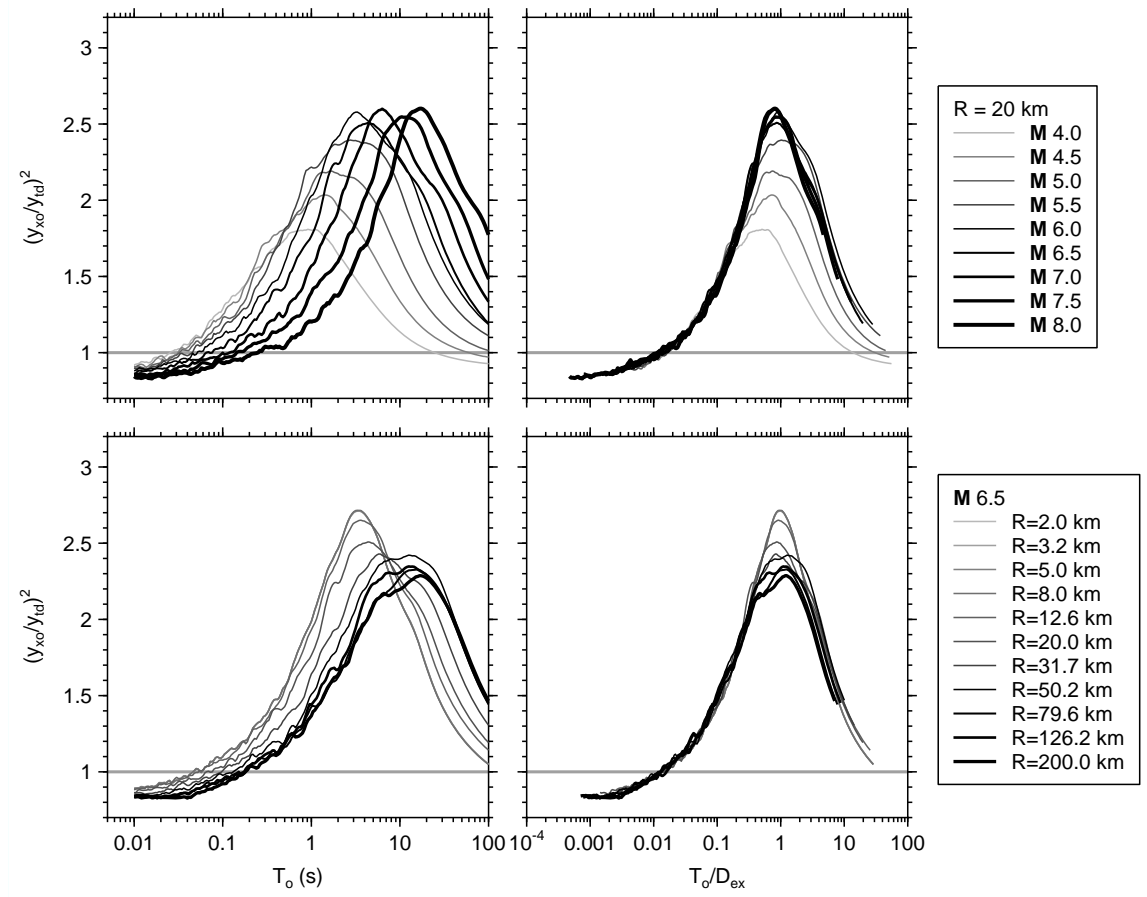


Figure 2. Squared ratios of PSA from random-vibration simulations (for which $D_{rms} = D_{ex}$) and time-domain simulations, for the ENA SCF model in Table 1 with 250 bar stress parameter and no low-cut filter, plotted against period (T_o) and period normalized by the duration of excitation (T_o/D_{ex}). The top row shows ratios for a fixed

distance (20 km) and a suite of magnitudes; the bottom row shows ratios for a fixed magnitude (6.5) and a suite of distances.

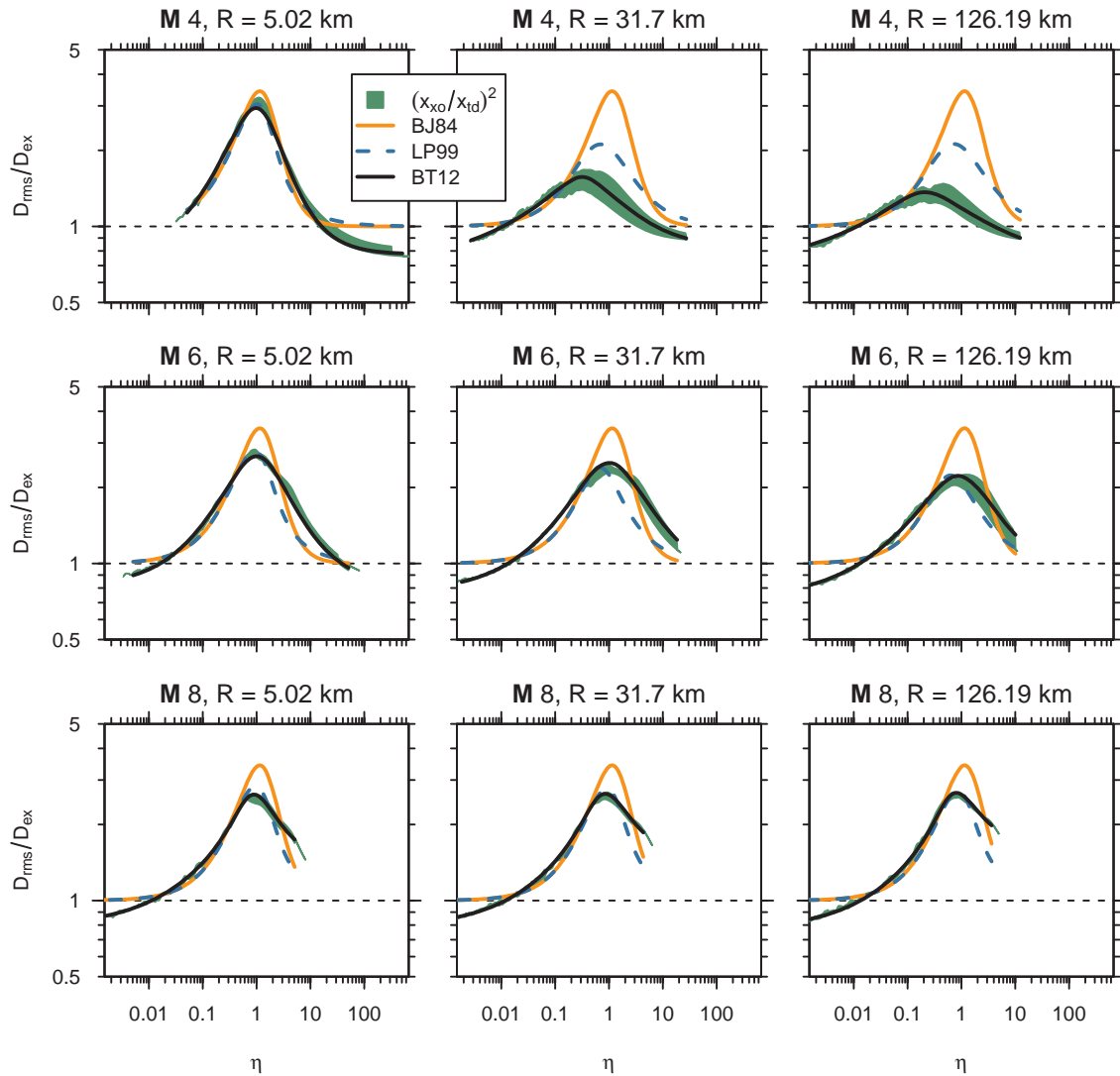


Figure 3. Plots of D_{rms}/D_{ex} as estimated from equation (6) (i.e., $(y_{xo}/y_{id})^2$) as a function of $\eta = T_o/D_{ex}$ for the same \mathbf{M} , \mathbf{R} , and stresses as Figure 1. The BT12 curves are from equation (10) with coefficients derived from fitting the D_{rms}/D_{ex} values derived from

the TD and RV simulations. The BJ84 and LP99 curves are from equation (8), with the coefficients recommended by the respective authors.

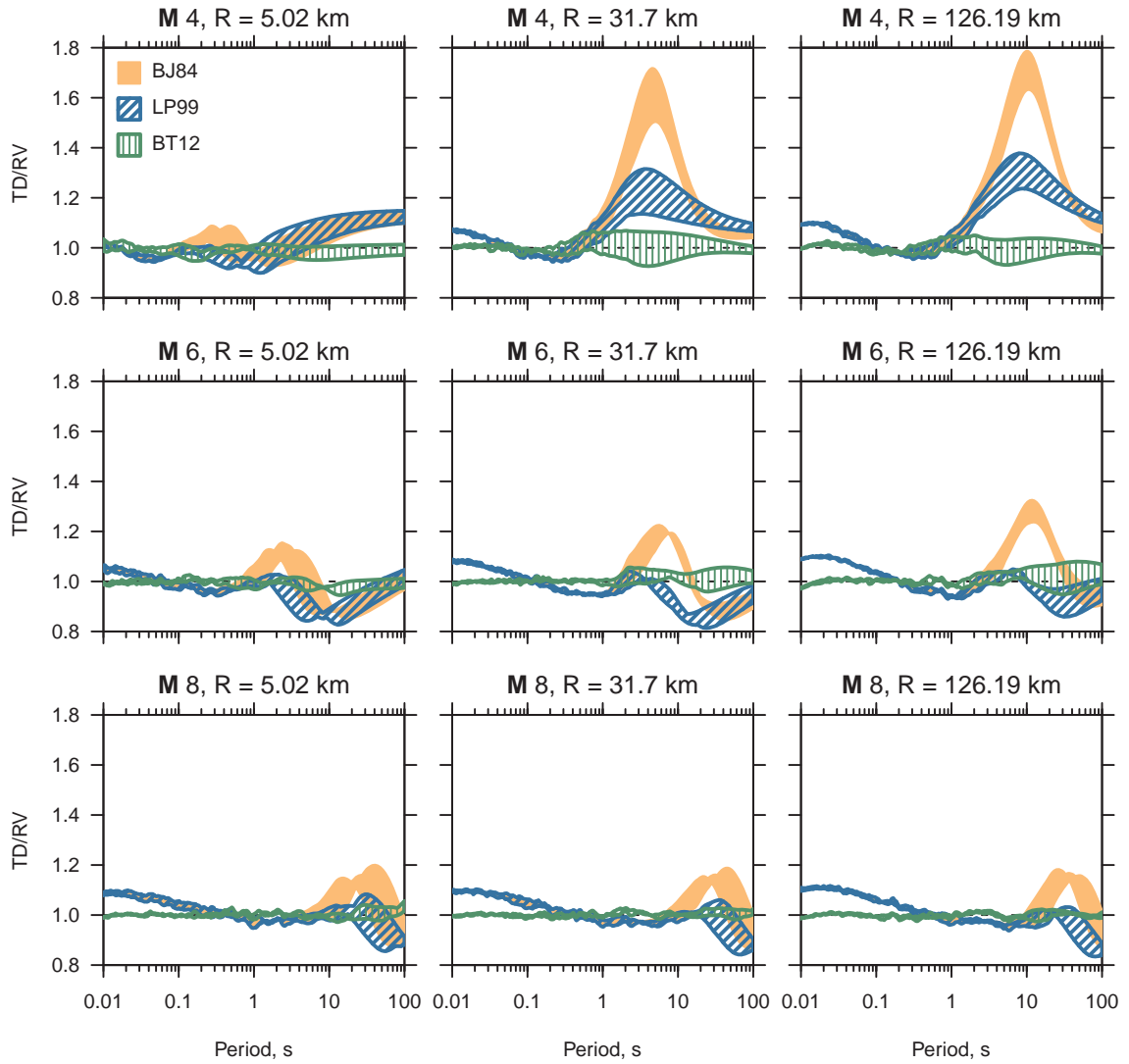


Figure 4. Same as Figure 1 with the addition of the ratios computed using the D_{rms} equation proposed in this article (BT12).

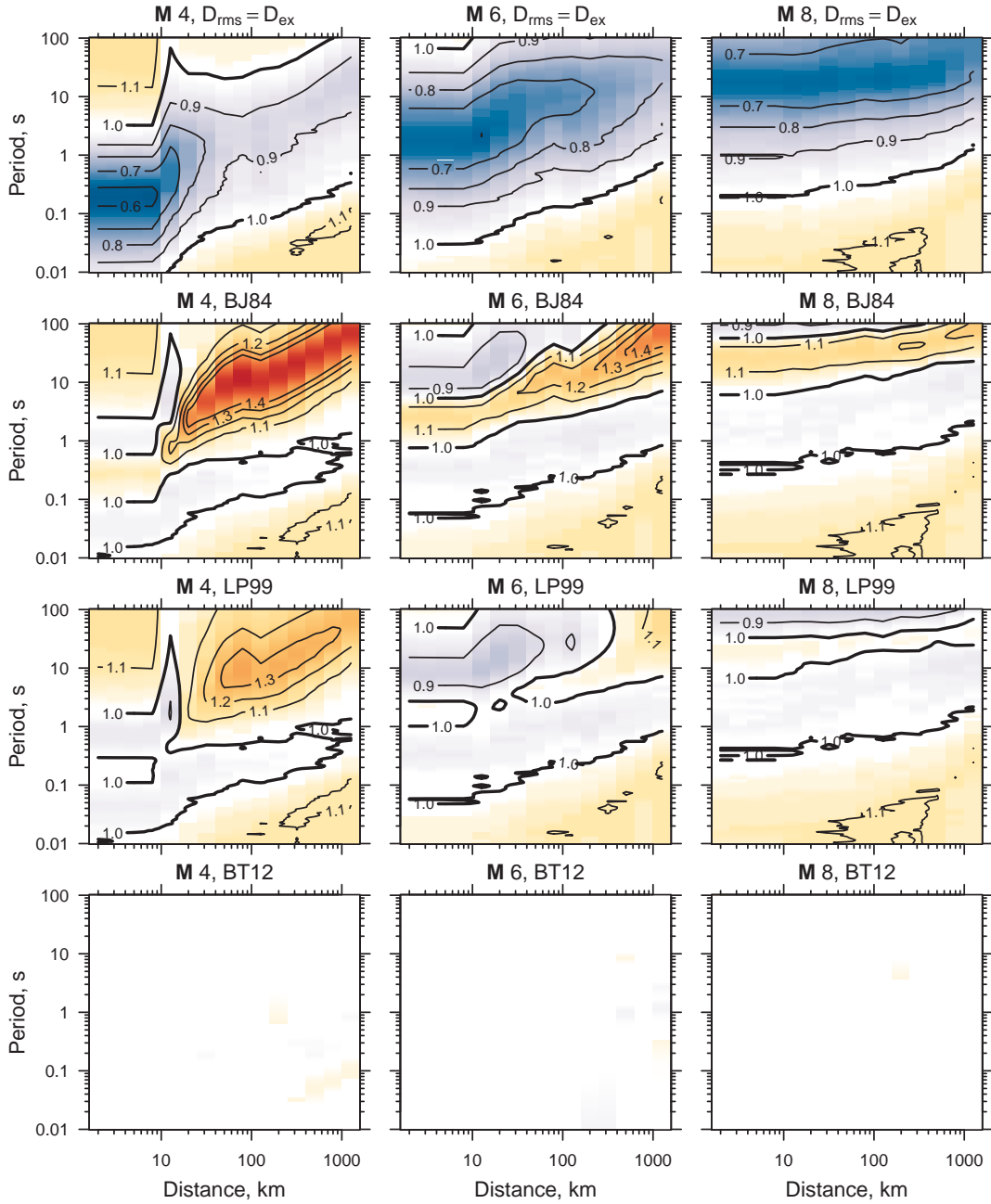


Figure 5. A shaded contour plot of the TD/RV ratios for the ENA SCF 250 bar, no low-cut filter model, for $D_{rms} = D_{ex}$ (no modification for an oscillator) (top row), and the following models for calculating the D_{rms} used in the RV simulations: BJ84 (second row),

LP99 (third row), and BT12 (bottom row). The results of using the BT12 calculations of D_{rms} look blank because the ratios are within $\pm 5.3\%$ of unity.

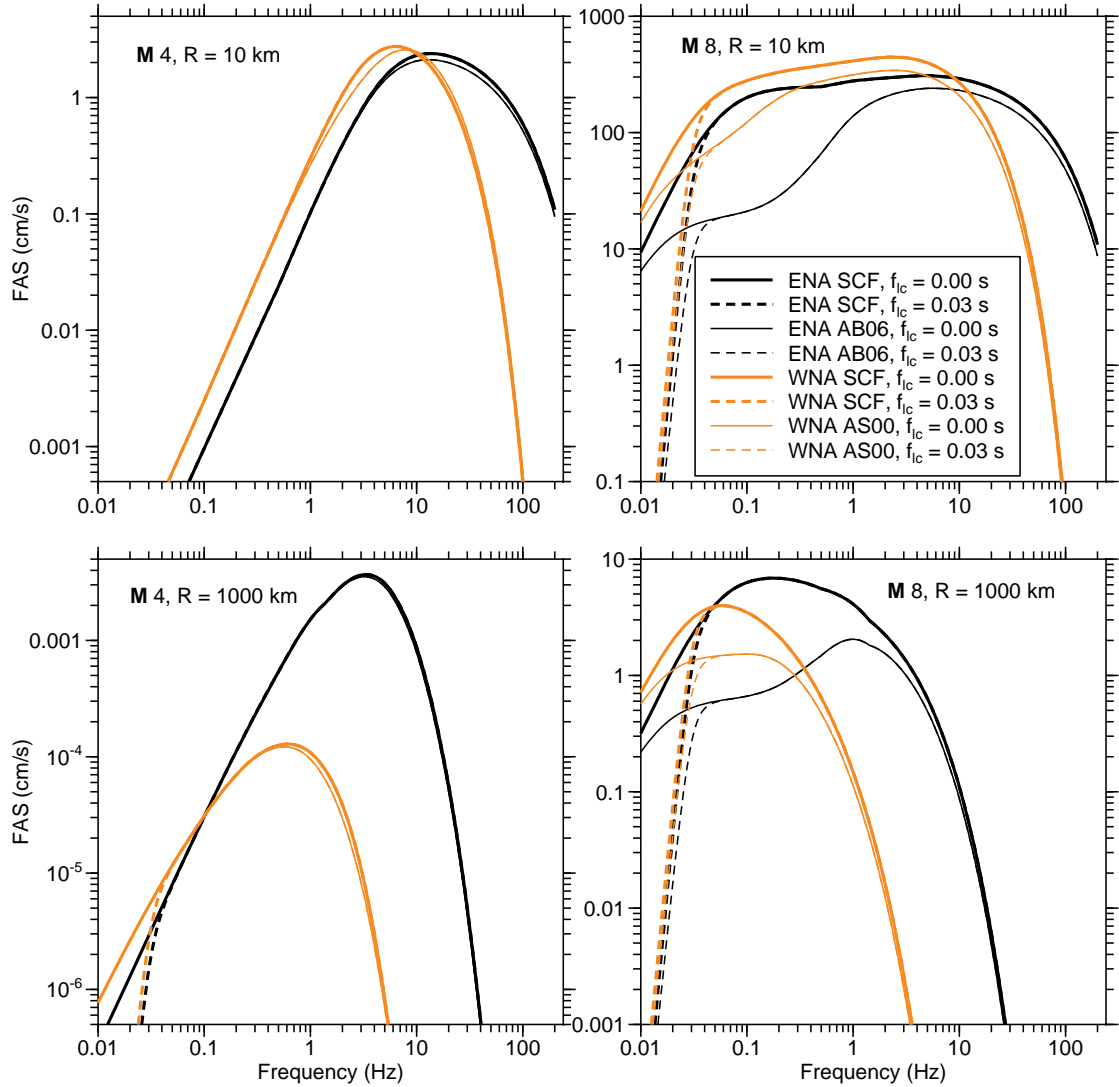


Figure 6. Fourier acceleration spectra (FAS) for models used in this article (see Table 1 and the electronic supplement to this paper), for selected magnitudes and distances.

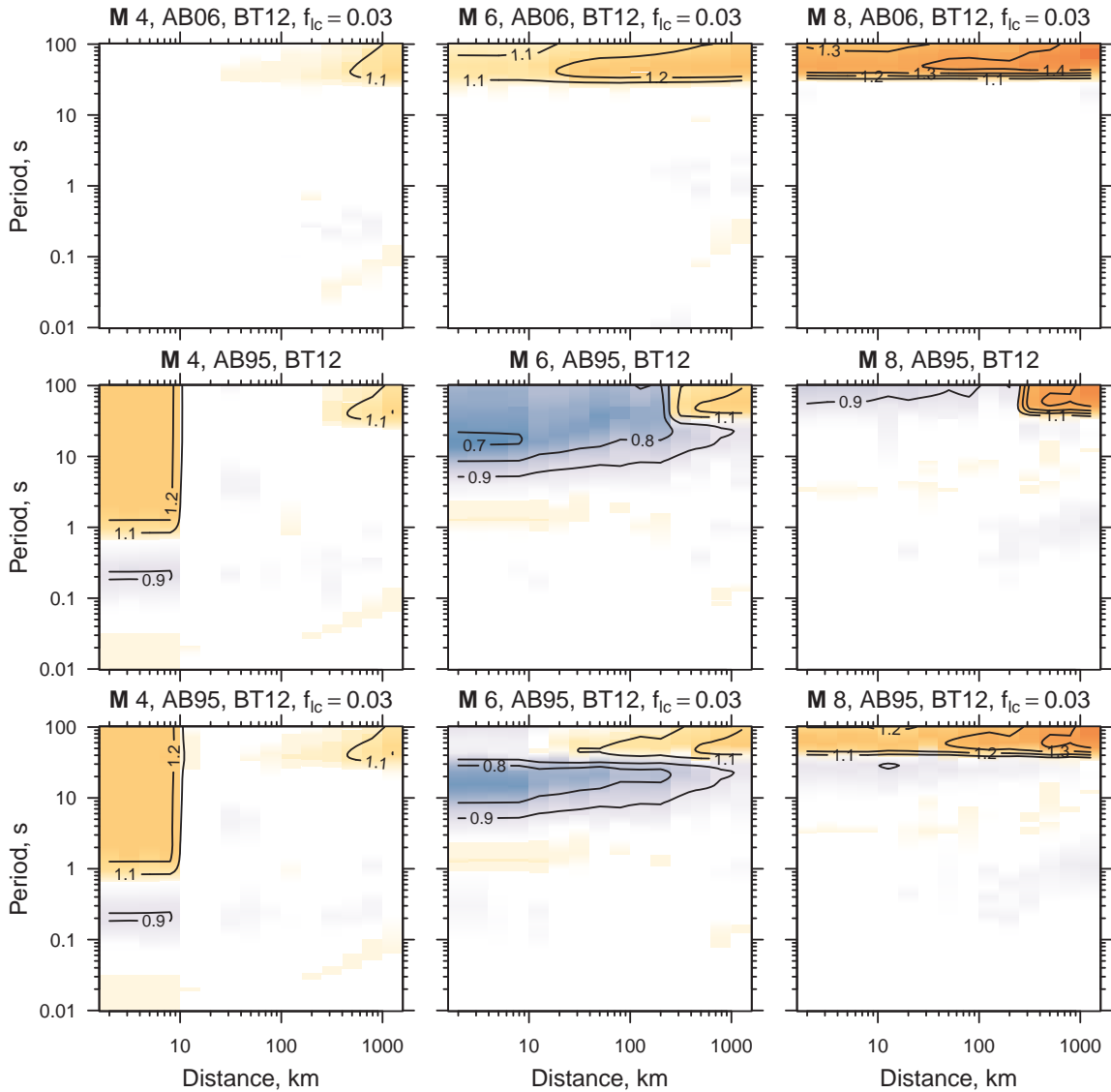


Figure 7. A shaded contour plot of the TD/RV ratios for various ENA models not used to derive the coefficients used in the BT12 D_{rms} computations (see Table 1 and the electronic supplement to this paper for model details). The base-case ENA BT12 coefficients were used in these comparisons. (top row): ENA SCF 250 bar model with a

0.03 Hz low-cut filter. (middle row): ENA AB95 two-corner model, no low-cut filter.
 (bottom row): ENA AB95 two-corner model, 0.03 Hz low-cut filter.

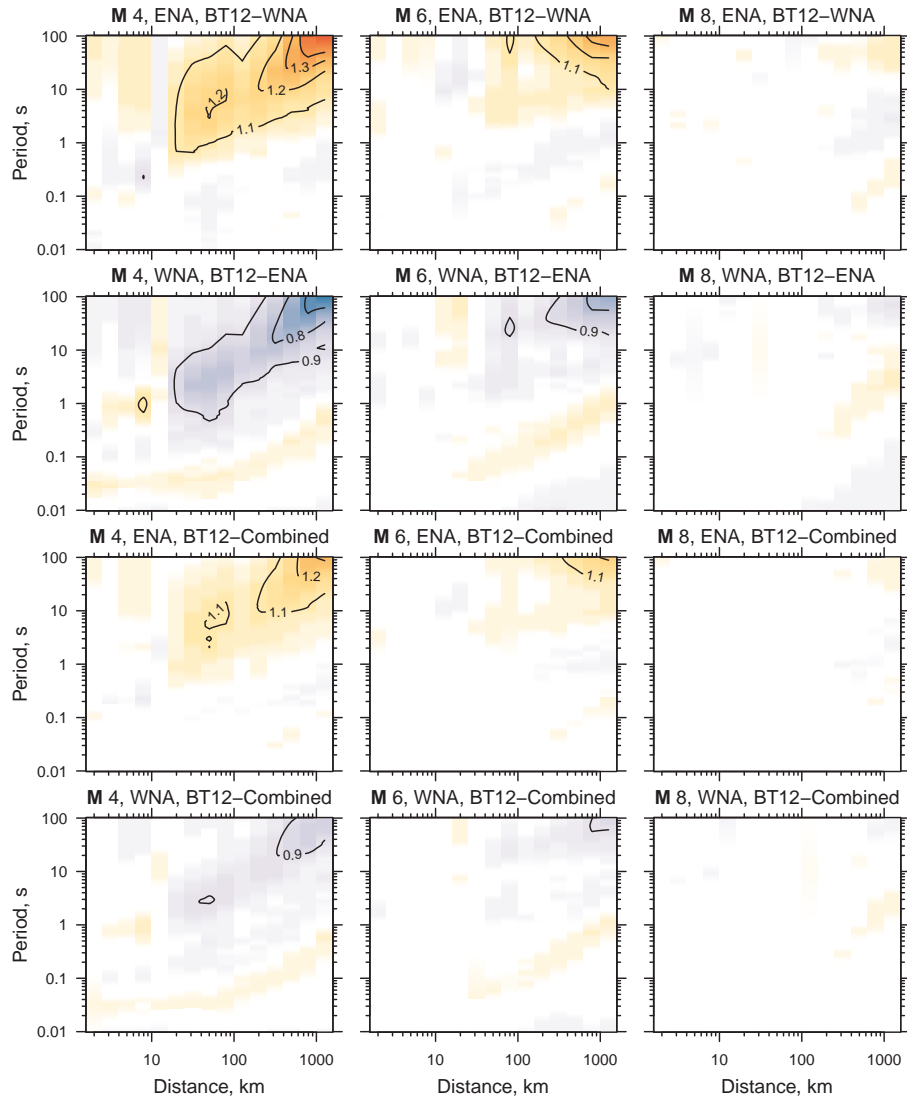


Figure 8. A shaded contour plot of the TD/RV ratios for various ENA and WNA models not used to derive the coefficients used in the BT12 D_{rms} computations (see Table 1 and the electronic supplement to this paper for model details). (top row): ENA SCF 250 bar model with no low-cut filter, using D_{rms} computed from the BT12 WNA coefficients. (second row): WNA SCF 100 bar model with no low-cut filter, using

D_{rms} computed from the BT12 ENA coefficients. (third row): ENA SCF 250 bar model with no low-cut filter, using an average of D_{rms} computed from the BT12 ENA and WNA coefficients. (bottom row): WNA SCF 100 bar model with no low-cut filter, using an average of D_{rms} computed from the BT12 ENA and WNA coefficients.